



The Pacific Decadal Oscillation modulated marine heatwaves in the Northeast Pacific during past decades

Xianglin Ren ^{1✉}, Wei Liu ¹, Antonietta Capotondi ², Dillon J. Amaya ² & Neil J. Holbrook ^{3,4}

The Pacific Decadal Oscillation has been suggested to play an important role in driving marine heatwaves in the Northeast Pacific during recent decades. Here we combine observations and climate model simulations to show that marine heatwaves became longer, stronger and more frequent off the Northeast Pacific coast under a positive Pacific Decadal Oscillation scenario, unlike what is found during a negative Pacific Decadal Oscillation scenario. This primarily results from the different mean-state sea surface temperatures between the two Pacific Decadal Oscillation phases. Compared to the cool (negative) phase of the Pacific Decadal Oscillation, warmer coastal sea surface temperatures occur during the positive Pacific Decadal Oscillation phase due to reduced coastal cold upwelling and increased net downward surface heat flux. Model results show that, relative to the background anthropogenic global warming, the positive Pacific Decadal Oscillation in the period 2013–2022 prolongs marine heatwaves duration by up to 43% and acts to increase marine heatwaves annual frequency by up to 32% off the Northeast Pacific coast.

¹Department of Earth and Planetary Sciences, University of California Riverside, Riverside, CA, USA. ²Physical Science Laboratory, Earth System Research Laboratory, National Oceanic and Atmospheric Administration, Boulder, CO, USA. ³Institute for Marine and Antarctic Studies, University of Tasmania, Hobart 7001 TAS, Australia. ⁴Australian Research Council Centre of Excellence for Climate Extremes, University of Tasmania, Hobart 7001 TAS, Australia. ✉email: xren024@ucr.edu

Heatwaves in the ocean, dubbed marine heatwaves (MHWs), are characterized by prolonged periods of extreme warm sea surface temperatures (SSTs) and are well known for adverse ecological and socio-economic impacts^{1–8}. Notable MHWs have recently been reported from various regions of the globe^{9–12}. In particular, a prominent MHW event developed during the winter of 2013–2014 in the Northeast Pacific, featuring unusually high SSTs in a “Blob-like” pattern in the Gulf of Alaska^{13,14}. During the following winter, the patch of warm water shifted from the Gulf of Alaska toward the coastal regions^{15,16}. Off the southern California coast, the maximum SST anomalies exceeded 5 °C relative to the 1982–2011 climatology. This MHW had significant impacts on marine ecosystems¹⁷ including harmful algal blooms¹⁸ and dramatic range shifts of species at all trophic levels^{19,20}. More recently, warm SST anomalies intensified in the Northeast Pacific^{21–25} in the summer of 2019.

A variety of physical mechanisms have been proposed to explain the occurrences of Northeast Pacific MHWs^{3,26,27}; for example, changes in the North Pacific high pressure system^{13,21}, the presence of El Niño conditions in the tropical Pacific^{15,28–31} and the North Pacific Gyre Oscillation (NPGO)¹⁴. We note here that both MHW events occurred since 2013 when the Pacific Decadal Oscillation (PDO)^{32,33} became positive³⁴, whereas few MHW events were reported in the prior decade or the so-called global warming hiatus period when the PDO was in a negative phase^{35–37}. This fact suggests the potential importance of the PDO for decadal variations of Northeast Pacific MHWs^{26,38}, especially when considering an inherent coupling between the NPGO and the subsequent development of PDO conditions³⁹. Although the importance of the PDO for the development of MHWs was previously discussed on the basis of statistical analysis^{26,38,39}, the role of the PDO in modulating decadal variations of Northeast Pacific MHWs and the associated physical mechanisms have not yet been explicitly investigated within fully coupled Earth’s system models. These aspects are then the focus of the current study.

Results

Observed decadal variations of Northeast Pacific MHWs. To explore the effect of the PDO on decadal variations of MHWs in the Northeast Pacific, we first examine the observed MHW changes (see Methods) over this region averaged over two positive PDO periods (1982–1998 and 2013–2022) and during a negative PDO period (1998–2013). We find that MHWs show generally longer (shorter) duration, higher (lower) annual frequency and larger (smaller) intensity off the Northeast Pacific coast during positive (negative) PDO periods (Fig. 1b–j). These robust MHW variations potentially reflect the effect of the PDO, but could also be influenced by many other factors. For example, the extent of background anthropogenic global warming could be different between 1982–1998 and 1998–2013, or between 1998–2013 and 2013–2022. We also note that negative PDO conditions appeared during 2020–2022 (Fig. 1a, Supplementary Fig. 1), suggesting that the positive PDO phase during 2013–2022 may have been short-lived. Finally, given that these results are based on only two positive PDO phases and one negative PDO phase, a more robust sample size is needed to confirm the relationships seen in Fig. 1.

Northeast Pacific MHWs during positive and negative PDO phases. To compare MHWs between two distinct PDO phases from many different samples, we calculate the frequency, duration and intensity of MHWs in the Northeast Pacific during 2013–2022 for the positive and negative PDO groups obtained

from the large ensemble simulations of five climate models (see Methods, Supplementary Fig. 2). While internal variability in each ensemble member has its own phase, here we consider the ensemble members which are in either a positive or negative PDO phase during 2013–2022 (see Methods). Like in observations, the MHW statistics from either group include the signals due to background anthropogenic forcing, whereas the difference between the two groups excludes the influence of background anthropogenic global warming (Fig. 2). Compared to the negative PDO group, the duration and annual frequency of MHWs in the Northeast Pacific significantly increase in the positive PDO group. From the Gulf of Alaska to off the California coast, MHW duration increases by about 3 days to 13 days (Fig. 2c) and MHW frequency enhances by about 0.4 to 1.1 times per year (Fig. 2f). MHWs also become significantly stronger off the coast of the Northeast Pacific in the positive PDO phase, except at a few sites in the Gulf of Alaska and close to Baja California (Fig. 2i). These model results, which are based on the comparison of robustly defined positive and negative PDO phases, are consistent with observations, indicating a role for the PDO in modulating Northeast Pacific MHWs during the recent decade, even if the PDO did not remain positive for the entire 2013–2022 period. Furthermore, we repeat our model analysis over two earlier decades, 1986–2005 (representing the positive PDO period of 1982–1998) and 1998–2007 (representing the negative PDO period of 1998–2013) and find that the PDO effects on MHWs during these two periods (Supplementary Figs. 3 and 4) are generally consistent with those in the period 2013–2022 (Fig. 2).

We also elucidate the PDO effect on warm SST extremes in the Northeast Pacific coastal region in terms of probability density functions (PDFs). We first calculate the PDF of daily SSTs over 2013–2022 with an interval of 0.1 °C for all ensemble members that exhibit either a positive or negative PDO during that period across the five climate models (Fig. 3a). We find that the SST PDF of all ensemble members has a mean of 15.4 °C. The PDF shows the SST pattern under background anthropogenic global warming, since the simulated PDO phase is random in the large ensemble simulations so that all of the internal variability in the different ensemble members cancels out. As a result, the PDF based on all the ensembles shows SST variations without preferred PDO phase (Supplementary Fig. 2a). On the other hand, the daily SSTs in the negative and positive PDO groups show mean changes of –0.8 °C and 0.9 °C, with PDFs skewed toward their lower and higher tails (the skewnesses are –0.44 °C³ and 0.37 °C³), respectively. These PDF patterns reflect the characteristics of SST changes due to anthropogenic global warming plus a preferred negative or positive PDO. The difference of the PDFs of the two PDO groups accordingly manifests the role of the PDO in modulating the daily SSTs in this region. By defining warm SST extremes here as those that exceed the 90th percentile, we find that the positive PDO phase significantly increases the likelihood of a warm extreme, or potentially, an MHW occurrence off the Northeast Pacific coast (Fig. 3a). However, the duration criterion also needs to be met. This result is consistent with observations at Monterey Bay⁴⁰, indicating that different PDO phases can alter the temperature and fertilization of near-shore surface water and potentially induce dramatic but distinct changes in coastal ecosystems and fisheries in the California Current region^{41–43}.

The physical mechanisms of the PDO in modulating MHWs. The distinct MHW statistics during positive and negative PDOs from SST PDF analysis can be attributed to different mean-state SSTs between the two PDO phases. This dependence of MHW characteristics on decadal-mean SSTs during different phases of

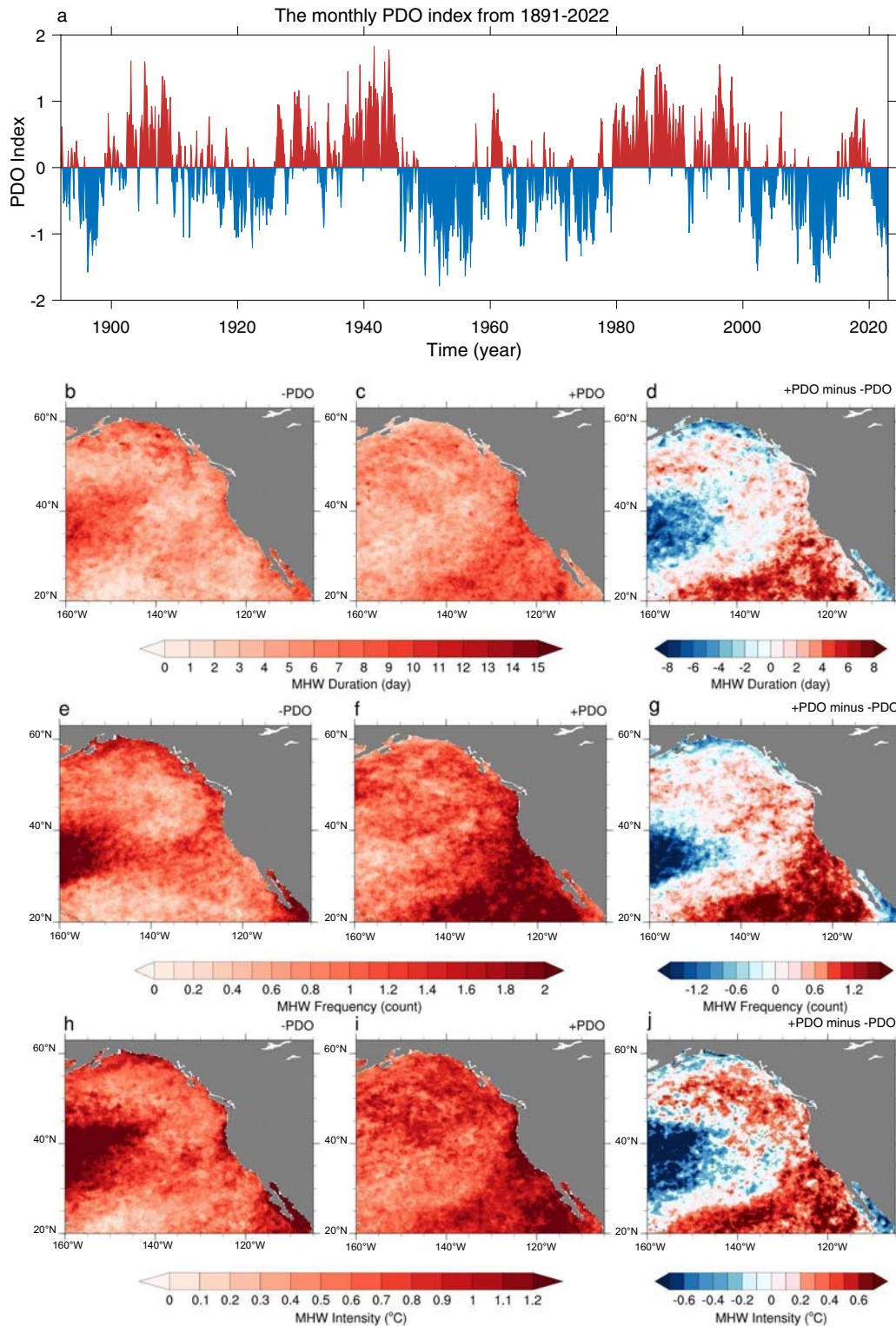


Fig. 1 Observed decadal variations of North Pacific MHWs. **a** The monthly PDO index from 1891–2022 for the average of COBE-SST, COBE-SSTv2, ERSSTv5 and HadISST. **b–d** North Pacific MHW duration averaged over **(b)** 1998–2013 and averaged over the combined periods of **(c)** 1982–1998 and 2013–2022 as well as **(d)** the difference between the two (**c** minus **b**). The average is applied on each grid. **e–g** Same as **(b–d)** but for annual MHW frequency. **h–j** Same as **(b–d)** but MHW intensity.

climate variability is consistent with the MHW dependence on the long-term SST state under climate change⁴⁴. Here, we calculate the difference of the 2013–2022 SST trend between the positive and negative PDO groups (Fig. 3b) and find contrasting SST changes in the western and central Pacific and along the

coast of the Northeast Pacific. The coastal SSTs exhibit an anomalous warming trend of 0.6–2.3 °C/year during a positive PDO phase as compared to a negative PDO phase.

We propose two physical mechanisms that can potentially drive the warmer coastal SST during a positive PDO. Compared

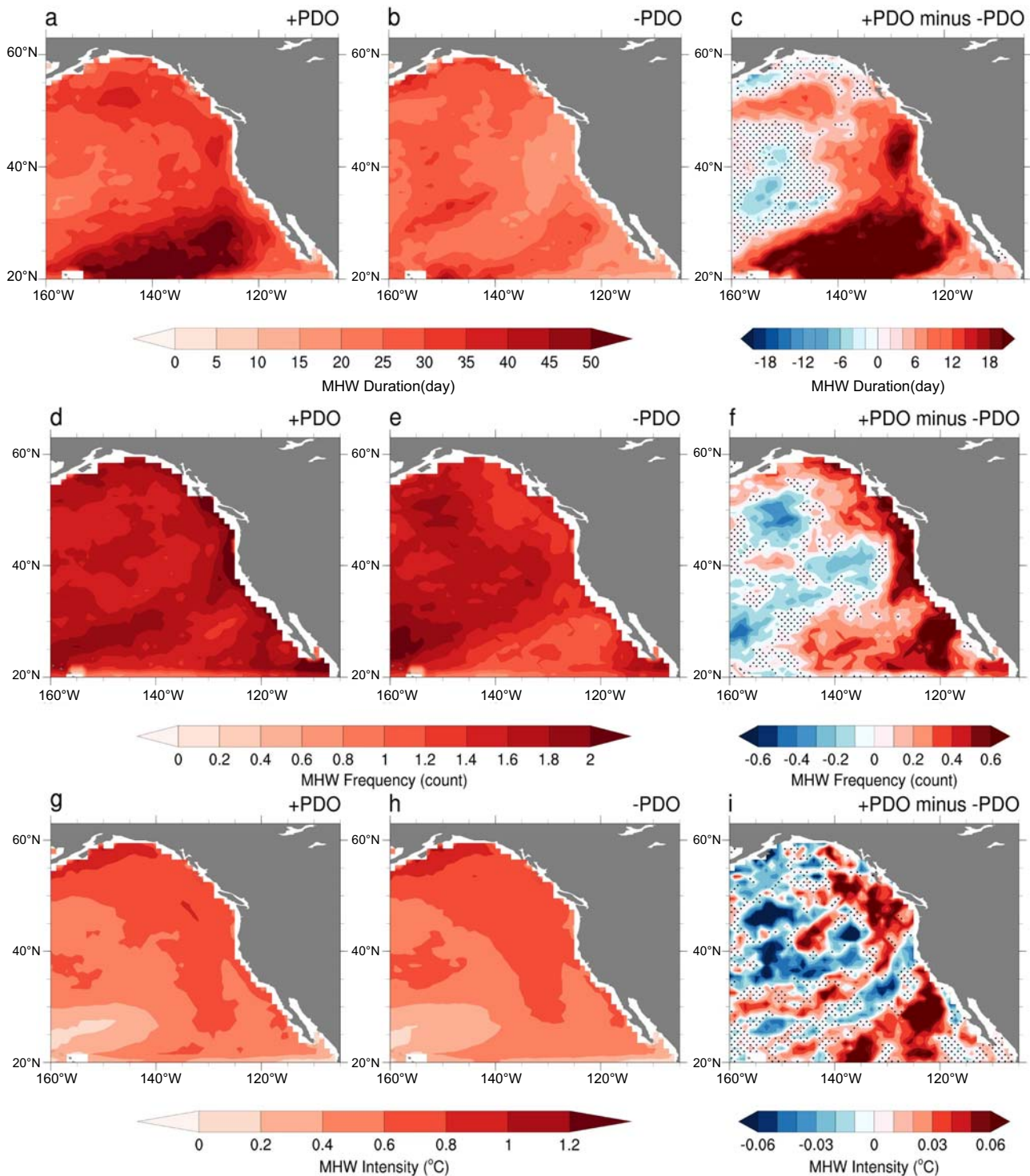


Fig. 2 Positive and negative PDOs modulating North Pacific MHWs. **a–c** Composite duration of Northeast Pacific MHWs for the ensemble mean of the **(a)** positive and **(b)** negative PDO groups from the large ensemble simulations of five climate models during 2013–2022 as well as **(c)** the difference between the two **(a, b)**. **d–f** Same as **(a–c)** but for annual MHW frequency. **g–i** Same as **(a–c)** but for MHW intensity. Dotted indicates that the change is not significantly different from zero at the 95% level of the Student's *t*-test.

to a negative PDO, anomalous surface southeasterly winds prevail along the coast of the Northeast Pacific during a positive PDO (Fig. 3b), which produce anomalous downward Ekman pumping (Fig. 3c), reduce the upwelling of cold water, and result in warmer coastal SSTs. Note that climate variability over the tropical Pacific can also remotely affect this region via the propagation of coastal Kelvin waves^{45,46}, whose offshore scale decreases with latitude.

These coastal waves can excite westward propagating Rossby waves, and thus affect the offshore regions, but the Rossby waves decay rapidly away from the coast⁴⁷, especially at higher latitudes where their phase speed is lower. Besides, more atmospheric heat enters through the ocean surface along the coast of the Northeast Pacific during a positive PDO (Fig. 3d). This increased net downward surface heat flux is primarily due to

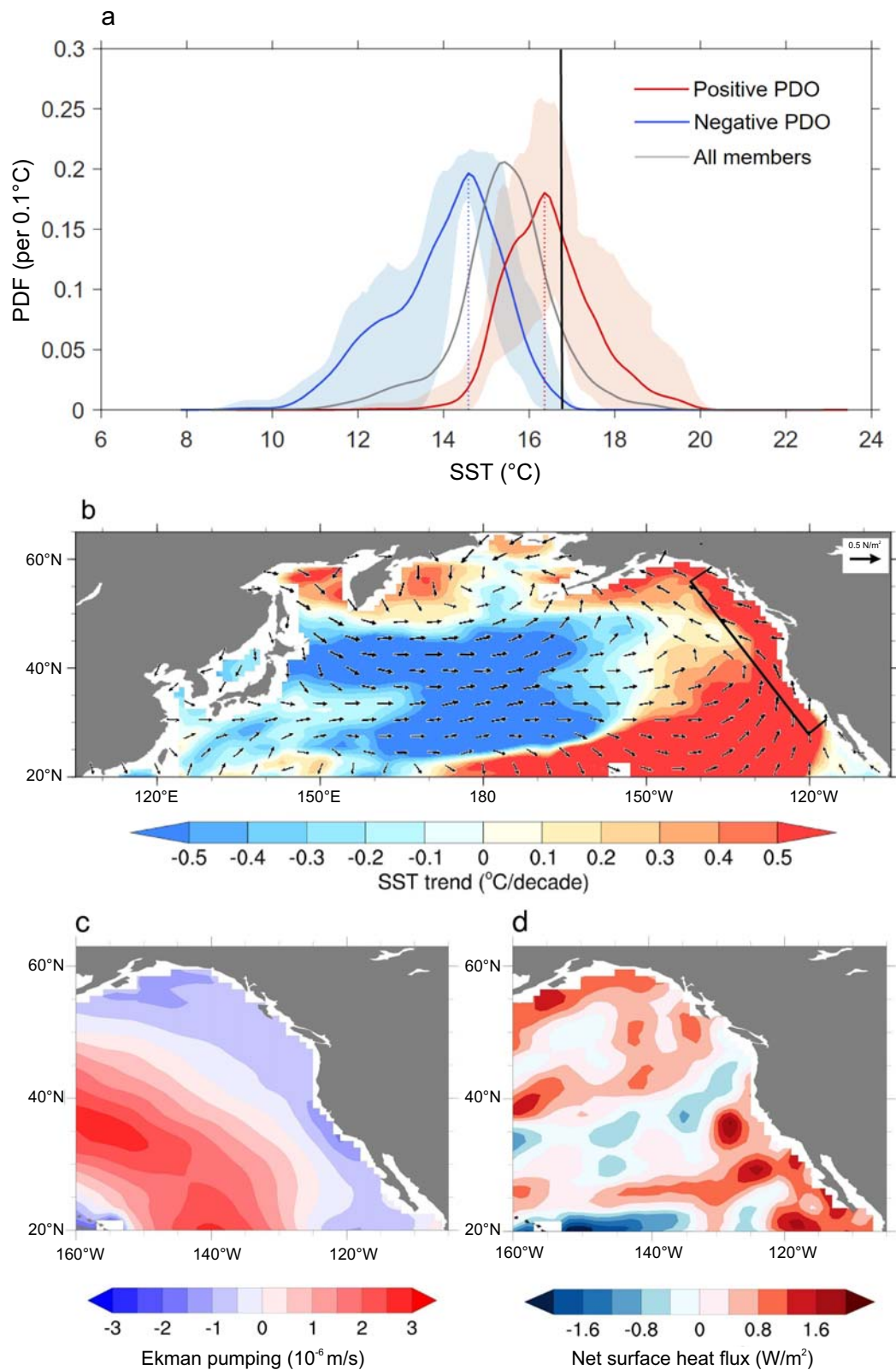


Fig. 3 The mean-state difference and the physical mechanisms. **a** Probability density functions (PDFs) of SSTs in the coastal region of the Northeast Pacific (within the enclosed area in **b**) during 2013–2022 for all ensemble members (gray), the positive (ensemble mean, red; ensemble spread, light red) and negative (ensemble mean, blue; ensemble spread, light blue) PDO groups from the five climate models simulations. The 90th percentile of the PDF from all ensemble members is denoted by the black line. The ensemble spread is defined as one standard deviation among the ensembles. **b** The differences of SST trend (shading) and surface wind stress (vector) during 2013–2022 between the positive and negative PDO groups (positive minus negative) for the ensemble mean of the five climate models. **c, d** Same as **(b)** but for the difference of Ekman pumping and net surface heat flux. Surface heat flux is downward positive.

enhanced downward shortwave radiation and diminished upward sensible and latent heat fluxes (Supplementary Fig. 5). The latter, reduced turbulent sensible and latent heat fluxes, could be related to the anomalous surface winds that weaken the climatological winds, and in turn, decrease the surface wind speed. Noting here, relative to the negative phase of the PDO, changes in the Ekman pumping and net surface heat flux amount to 28% and 24% in magnitude during the positive phase of the PDO, which are sufficiently strong to alter the decadal-mean SSTs and impact the characteristics of MHWs. To summarize, both surface heat flux changes and ocean dynamics are important to the generation of warmer mean-state SST and hence longer, stronger and more frequent MHWs along the coast of the Northeast Pacific during a positive PDO.

We further quantify the PDO effect on Northeast Pacific MHWs during 2013–2022 by comparing it against the relative background anthropogenic global warming (Fig. 4a–c; Eqs. 1 and 2; also see Methods). We find that a positive PDO can prolong the MHW duration by up to 43%, increase the MHW annual frequency by up to 32%, and enlarge the MHW intensity by up to 10% off the Northeast Pacific coast (Fig. 4d–f). On the other hand, a negative PDO can shorten the MHW duration by up to 38%, decrease the MHW annual frequency by up to 29%, and reduce the MHW intensity by up to 10% in this region (Fig. 4g–i).

Discussion

In this study, we have explored the role of the PDO in driving MHWs in the Northeast Pacific on decadal timescales using both observations and climate model simulations. We find that, over recent decades, MHWs off the coast of the Northeast Pacific have become longer, more intense and more frequent under a positive PDO scenario relative to what is seen during a negative PDO scenario. These results are confirmed by the comparison of MHW statistics during positive and negative PDO conditions obtained from five climate models large ensembles. Analyses of these climate models reveal that these distinct MHW characteristics primarily resulted from the different mean-state SSTs between the two PDO phases. Compared to the negative phase of the PDO, warmer SSTs occur along the Northeast Pacific coast during the positive PDO, which are generated by suppressed coastal cold upwelling and enhanced net downward surface heat flux. We further quantify the contributions of the PDO and background anthropogenic global warming on Northeast Pacific MHWs over the past decade. Relative to background anthropogenic global warming, the positive PDO can prolong MHW duration by as much as 43% and act to increase MHW annual frequency by as much as 32% off the Northeast Pacific coast.

Our results suggest that periods of longer, stronger and more frequent Northeast Pacific MHWs can last for several years due to the persistence of a positive PDO state. Nevertheless, the characteristic MHW pattern induced by the positive PDO does not need to account for every event. For example, the “Blob” in February 2014 featured a peak warming centered around 145°W as likely related to the NPGO mode, which also makes sense in light of the inherent coupling between the NPGO and PDO³⁹. Moreover, besides the North Pacific, the PDO could also have a remote effect on the SST in the Gulf of Maine during spring and summer through atmospheric teleconnections⁴⁸ and potentially affect MHWs in the Northwest Atlantic.

The contribution of the PDO under the influence of background anthropogenic global warming on Northeast Pacific MHWs may change. As our climate continues to warm, the PDO is expected to weaken and to have a shorter period^{49–51}. The underlying cause is that global warming enhances the ocean stratification in the North Pacific⁵², which leads to increased

phase speed but decreased magnitude of extratropical oceanic Rossby waves across the North Pacific^{53,54}. The increased Rossby wave phase speed results in a shorter transit time and therefore reduced periodicity of the PDO, while the reduced Rossby wave amplitude leads to a weaker PDO relative to the present. This alteration in PDO characteristics may further affect the predictability of the PDO^{51,55}. It is also worth mentioning that, from an alternative point of view, the PDO is not a physical mode of variability like the El Niño-Southern Oscillation (ENSO). Rather, it is the result of the superposition of different processes, including ENSO teleconnections, re-emergence, and Rossby wave propagation in the North Pacific⁵³. Given that current global climate forecast systems have shown relatively limited skill in the prediction of MHWs⁵⁶ except for those linked to ENSO⁵⁷, improving the understanding of changes in ENSO and PDO predictability under climate change will be fundamental for assessing the potential predictability of MHWs on interannual to decadal timescales.

Methods

Observations. We exploit the Daily Optimum Interpolation Sea Surface Temperature (OISST) version 2.1 (v2.1) from the National Oceanic and Atmospheric Administration⁵⁸, mapped onto a $0.25^\circ \times 0.25^\circ$ grid and available since September 1, 1981. We adopt the OISST data from 1982 to 2022 to investigate the observed MHWs in the Northeast Pacific. To examine the historical PDO, we leverage multiple reconstructed monthly SST datasets: COBE-SST⁵⁹, COBE-SSTv2⁶⁰, ERSSTv5⁶¹ and HadISST⁶², which are generally of a resolution of one or two degrees and cover more than a century. For each dataset, we calculate the SST anomalies during the period from 1891–2022 by removing both the climatological annual cycle and the global-mean SST at each grid point. We determine the PDO structure using the leading empirical orthogonal function (EOF) of the SST anomalies in the North Pacific polewards of 20°N^{32,63} and compute the PDO index as the corresponding principal component of the leading EOF. Despite slight differences, all four reconstructed monthly SST datasets show consistent PDO structures and indices (Supplementary Fig. 1). We hence use the average of the four PDO indices when examining the historical PDO (Fig. 1a).

Climate model simulations. Previous studies^{3,26,27} suggest that many physical drivers, including the PDO, operate under background anthropogenic warming such that it is difficult to clearly isolate and quantify the effect of each driver simply using short-record observational data. To this end, we leverage large ensemble simulations with climate models to eliminate the influence of background anthropogenic global warming and identify the effect of the PDO. The underlying rationale is that the predictability horizon of climate models is at most one to two decades^{55,64,65} so that they may not capture the same timing of internal decadal climate variability as observations⁶⁴. For example, during the recent decade, 2013–2022, climate models can simulate the PDO in different phases among individual ensemble members but under the same anthropogenic forcing (Supplementary Fig. 2a). Thereby, the average of these large ensembles allows a cancellation between positive and negative PDOs and hence a representation of background anthropogenic global warming (Supplementary Fig. 2a). Meanwhile, a comparison between these members during different PDO phases will help uncover the role of the PDO in influencing various climate elements, including MHWs.

In this study, we consider large ensemble simulations conducted with five climate models that have daily SST outputs available: ACCESS-ESM1.5⁶⁶, CanESM5⁶⁷, CESM1⁶⁸, CESM2^{69,70}, and EC-Earth3⁷¹, i.e., we use 172 ensemble members in total (Supplementary Table 1). The model PDO is calculated using the same approach as for the observed PDO. For each ensemble member, we calculate its PDO index as the principal component of the leading EOF based on the simulated SST anomalies over the period 1920–2022. We adopt a similar approach to that in ref. ⁷² by selecting the ensemble members that simulate a positive (negative) PDO during 2013–2022 into a positive (negative) PDO group (Supplementary Fig. 2b, Supplementary Table 1). We calculate the difference for the ensemble means between the positive and negative PDO groups to explore the PDO effect on MHWs (Supplementary Fig. 2). Here, it is worth noting that, although the five models follow different future anthropogenic warming scenarios after 2005 or 2014 (Supplementary Table 1), the inter-model difference in external forcing between 2013–2022 is fairly small and seldom affects the result in the current study.

Besides 2013–2022, we also selected the ensemble members that simulated a positive (negative) PDO during two earlier decades—1986–1995 and 1998–2007—into positive (negative) PDO groups, respectively (Supplementary Fig. 2c, d, Supplementary Table 2). For either decade, we calculated the difference in the ensemble means between the positive and negative PDO groups to explore the PDO effect on MHWs (Supplementary Figs. 3 and 4).

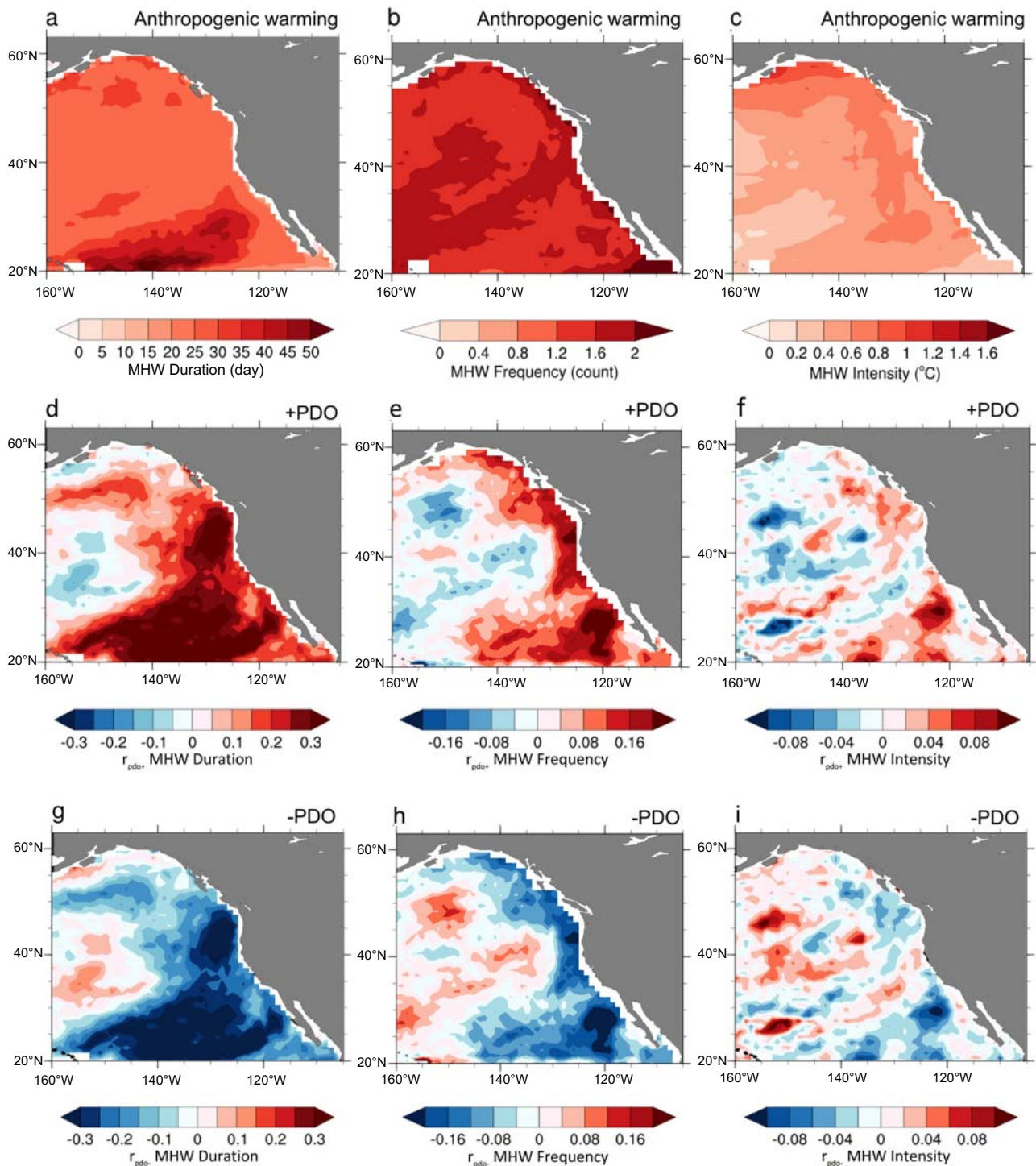


Fig. 4 Quantifications of the PDO effect on North Pacific MHWs. **a–c** The ensemble mean of (a) duration, (b) annual frequency and (c) intensity of Northeast Pacific MHWs during 2013–2022 for all ensemble members from the five climate models simulations, which reveals the effect of background anthropogenic global warming during the decade (\overline{MHW}_{agr} ; see Methods). **d–f** The ensemble mean of r_{pdo+} (see Methods) for (d) duration, (e) annual frequency, and (f) intensity of Northeast Pacific MHWs during 2013–2022 for the five climate models simulations. **g–i** Same as (d–f) but for the ensemble mean of r_{pdo-} (see Methods).

Detection of marine heatwaves. We adopt the MHW definition from ref. ⁷³ in which a MHW represents an event in which daily SST exceeds the local seasonal threshold (i.e., the 90th percentile of daily SST for the same day during the climatology period) for at least five consecutive days within a given area. Two events with an interruption of <3 days are considered as one MHW event. For observations, we probe the MHWs during 1982–2022 using OISSTv2.1 so that the climatological period for MHW detection is 1982–2022. For climate model simulations, we focus on the PDO effect on MHWs during the recent decade. For

each model, we use ensemble mean daily SST climatology during 2013–2022 for MHW detections. Though this 2013–2022 climatology or the neutral PDO state lasts only one decade, our ensemble mean approach in model simulations helps capture the background anthropogenic warming and allows for a better representation of daily SST climatology under global warming⁷⁴. Similarly, we use ensemble mean daily SST climatology during 1986–1995 or 1998–2007 for MHW detections in either period. For all the reference periods in both observations and model simulations, the daily SST climatology and the 90th percentile threshold

corresponding to each day are calculated using the daily SST for all years within 11 days centered on that day, and the results obtained are then smoothed for 31 days.

We explore MHW characteristics such as frequency, duration and intensity from observations and model simulations. Frequency is defined as the number of events per year; duration is defined as the time between the start date and end date of the event; and intensity is defined as the maximum amplitude of each MHW, i.e., the maximum SST anomaly relative to the seasonally varying climate mean over the duration of the event. We apply the Student's *t*-test to the difference of MHW characteristics between positive and negative PDO groups to examine the statistical significance of the PDO effect on MHWs.

To quantify the PDO effect on Northeast Pacific MHWs during 2013–2022, we first calculate MHW duration, frequency and intensity averaged over all the ensembles of the five models (\overline{MHW}_{agw}), which reveals the effect of background anthropogenic global warming during the decade. We then calculate MHW duration, frequency and intensity averaged over the ensembles of the positive (\overline{MHW}_{pdo+}) and negative (\overline{MHW}_{pdo-}) groups. Relative to the background anthropogenic global warming, the effects of the positive and negative PDOs on MHWs can be denoted by the ratios of r_{pdo+} and r_{pdo-} , i.e.,

$$r_{pdo+} = (\overline{MHW}_{pdo+} - \overline{MHW}_{agw}) / \overline{MHW}_{agw} \quad (1)$$

$$r_{pdo-} = (\overline{MHW}_{pdo-} - \overline{MHW}_{agw}) / \overline{MHW}_{agw} \quad (2)$$

Data availability

OISST v2.1 data are publically available at <https://www.ncdc.noaa.gov/oisst/optimun-interpolation-sea-surface-temperature-oisst-v2.1>. ERSSTv5 data are publically available at <https://www.noaa.gov/pub/data/cmb/ersst> (noaa.gov). COBA-SST& COBA-SSTv2 data are publically available at Global Sea Surface Temperature Data Sets/TCC (jma.go.jp). HadISST1.1 data are publically available at CISL RDA: Hadley Centre Global Sea Ice and Sea Surface Temperature (HadISST) (ucar.edu). The outputs of CESM1 and CESM2 simulations are publically available at CESM Large Ensemble Data Sets (ucar.edu). CESM2 Large Ensemble Data Sets (ucar.edu). The outputs of ACCESS-ESM1.5, CanESM5 and EC-Earth3 simulations are publically available at <https://esgf-node.llnl.gov/projects/cmip6/>.

Code availability

The figures presented in this manuscript were conducted using The NCAR Command Language (Version 6.6.2) [Software]. (2019). Boulder, Colorado: UCAR/NCAR/CISL/TDD. <https://doi.org/10.5065/D6W3DXH5>.

Received: 2 December 2022; Accepted: 24 May 2023;

Published online: 19 June 2023

References

- Frölicher, T. L., Fischer, E. M. & Gruber, N. Marine heatwaves under global warming. *Nature* **560**, 360–364 (2018).
- Smale, D. A. et al. Marine heatwaves threaten global biodiversity and the provision of ecosystem services. *Nat. Clim. Change* **9**, 306–312 (2019).
- Holbrook, N. J. et al. Keeping Pace with Marine Heatwaves. *Nat. Rev. Earth Environ.* **1**, 482–493 (2020).
- Holbrook, N. J. et al. in *Changing Climate* (Eds. McPhaden, M. J., Santoso, A. & Cai, W.) Ch. 18 (American Geophysical Union (AGU), 2021).
- Oliver, E. C. J. et al. Marine Heatwaves. *Ann. Rev. Mar. Sci.* **13**, 313–342 (2021).
- Oliver, E. C. et al. Projected marine heatwaves in the 21st century and the potential for ecological impact. *Front. Mar. Sci.* **6**, 734 (2019).
- Smith, K. E. et al. Socioeconomic impacts of marine heatwaves: global issues and opportunities. *Science* **374**, eabj3593 (2021).
- Smith, K. E. et al. Biological impacts of marine heatwaves. *Ann. Rev. Mar. Sci.* **15**, 1 (2023).
- Garrabou, J. et al. Mass mortality in Northwestern Mediterranean rocky benthic communities: effects of the 2003 heat wave. *Glob. Change Biol.* **15**, 1090–1103 (2009).
- Chen, K., Gawarkiewicz, G. G., Kwon, Y.-O. & Zhang, W. G. The role of atmospheric forcing versus ocean advection during the extreme warming of the northeast U.S. continental shelf in 2012. *J. Geophys. Res. Oceans* **120**, 4324–4339 (2015).
- Chen, K., Gawarkiewicz, G. G., Lentz, S. J. & Bane, J. M. Diagnosing the warming of the northeastern U.S. coastal ocean in 2012: a linkage between the atmospheric jet stream variability and ocean response. *J. Geophys. Res. Oceans* **119**, 218–227 (2014).
- Oliver, E. C. J. et al. The unprecedented 2015/16 Tasman Sea marine heatwave. *Nat. Common.* **8**, 16101 (2017).
- Bond, N. A., Cronin, M. F., Freeland, H., & Mantua, N. Causes and impacts of the 2014 warm anomaly in the NE Pacific. *Geophys. Res. Lett.* **42**, 3414–3420 (2015).
- Di Lorenzo, E. & Mantua, N. Multi-year persistence of the 2014/15 North Pacific marine heatwave. *Nat. Clim. Change* **6**, 1042–1047 (2016).
- Jacox, M. G. et al. Impacts of the 2015–2016 El Niño on the California Current System: early assessment and comparison to past events. *Geophys. Res. Lett.* **43**, 7072–7080 (2016).
- Amaya, D. J., Bond, N. E., Miller, A. J. & DeFlorio M. J. in *A Tale of Two Blobs 1–6* (U.S. CLIVAR, 2016).
- Cavole, L. M. et al. Biological impacts of the 2013–2015 warm-water anomaly in the Northeast Pacific: winners, losers, and the future. *Oceanography* **29**, 273–285 (2016).
- McCabe, R. M. et al. An unprecedented coastwide toxic algal bloom linked to anomalous ocean conditions. *Geophys. Res. Lett.* **43**, 10366–10376 (2016).
- Peterson, W. T. et al. The pelagic ecosystem in the Northern California Current off Oregon during the 2014–2016 warm anomalies within the context of the past 20 years. *J. Geophys. Res. Oceans* **122**, 7267–7290 (2017).
- Sanford, E., Sones, J. L., García-Reyes, M., Goddard, J. H. & Largier, J. L. Widespread shifts in the coastal biota of northern California during the 2014–2016 marine heatwaves. *Sci. Rep.* **9**, 4216 (2019).
- Amaya, D. J., Miller, A. J., Xie, S.-P. & Kosaka, Y. Physical drivers of the summer 2019 North Pacific marine heatwave. *Nat. Common.* **11**, 1903 (2020).
- Amaya, D. J. et al. Are long-term changes in mixed layer depth influencing North Pacific Marine heatwaves? *Bull. Amer. Meteor. Soc.* **102**, S59–S66 (2021).
- Scannell, H. A., Johnson, G. C., Thompson, L., Lyman, J. M. & Riser, S. C. Subsurface evolution and persistence of marine heatwaves in the Northeast Pacific. *Geophys. Res. Lett.* **47**, e2020GL090548 (2020).
- Chen, Z., Shi, J., Liu, Q., Chen, H. & Li, C. A persistent and intense marine heatwave in the Northeast Pacific during 2019–2020. *Geophys. Res. Lett.* **48**, e2021GL093239 (2021).
- Shi, J. et al. Role of mixed layer depth in the location and development of the Northeast Pacific warm blobs. *Geophys. Res. Lett.* **49**, e2022GL098849 (2022).
- Holbrook, N. J. et al. A global assessment of marine heatwaves and their drivers. *Nat. Common.* **10**, 2624 (2019).
- Sen Gupta, A. et al. Drivers and impacts of the most extreme marine heatwave events. *Sci. Rep.* **10**, 1–15 (2020).
- Frischknecht, M., Münnich, M. & Gruber, N. Local atmospheric forcing driving an unexpected California Current System response during the 2015–2016 El Niño. *Geophys. Res. Lett.* **44**, 304–311 (2017).
- Capotondi, A., Sardeshmukh, P. D., Di Lorenzo, E., Subramanian, A. C. & Miller, A. J. Predictability of US West Coast Ocean Temperatures is not solely due to ENSO. *Sci. Rep.* **9**, 10993 (2019).
- Capotondi, A., Newman, M., Xu, T. & Di Lorenzo, E. An optimal precursor of Northeast Pacific Marine heatwaves and Central Pacific El Niño events. *Geophys. Res. Lett.* **49**, e2021GL097350 (2022).
- Xu, T., Newman, M., Capotondi, A. & Di Lorenzo, E. The continuum of Northeast Pacific marine heatwaves and their relationship to the Tropical Pacific. *Geophys. Res. Lett.* **48**, e2020GL090661 (2021).
- Zhang, Y., Wallace, J. M. & Battisti, D. S. ENSO-like interdecadal variability: 1900–93. *J. Clim.* **10**, 1004–1020 (1997).
- Mantua, N. J. et al. A Pacific interdecadal climate oscillation with impacts on salmon production. *Bull. Amer. Meteor. Soc.* **78**, 1069–1080 (1997).
- Johnson, N. C. et al. Multidecadal modulations of key metrics of global climate change. *Glob. Planet. Change* **188**, 103149 (2020).
- Kosaka, Y. & Xie, S.-P. Recent global-warming hiatus tied to equatorial Pacific surface cooling. *Nature* **501**, 403–407 (2013).
- Meehl, G. A., Hu, A., Arblaster, J. M., Fasullo, J. & Trenberth, K. E. Externally forced and internally generated decadal climate variability associated with the Interdecadal Pacific Oscillation. *J. Clim.* **26**, 7298–7310 (2013).
- Liu, W. & Xie, S.-P. An ocean view of the global surface warming hiatus. *Oceanography* **31**, 72–79 (2018).
- Scannell, H. A., Pershing, A. J., Alexander, M. A., Thomas, A. C. & Mills, K. E. Frequency of marine heatwaves in the North Atlantic and North Pacific since 1950. *Geophys. Res. Lett.* **43**, 2069–2076 (2016).
- Joh, Y. & Di Lorenzo, E. Increasing coupling between NPGO and PDO leads to prolonged marine heatwaves in the Northeast Pacific. *Geophys. Res. Lett.* **44**, 11663–11671 (2017).
- Chavez, F. P. et al. Climate variability and change: response of a coastal ocean ecosystem. *Oceanography* **30**, 128–145 (2017).
- Miller, A. J. & Schneider, N. Interdecadal climate regime dynamics in the North Pacific Ocean: theories, observations and ecosystem impacts. *Prog. Oceanogr.* **47**, 355–379 (2000).

42. Miller, A. J. et al. Potential feedbacks between Pacific Ocean ecosystems and interdecadal climate variations. *Bull. Amer. Meteor. Soc.* **84**, 617–633 (2003).
43. Miller, A. J. et al. Decadal-scale climate and ecosystem interactions in the North Pacific Ocean. *J. Oceanogr.* **60**, 163–188 (2004).
44. Oliver, E. C. J. et al. Longer and more frequency marine heatwaves over the past century. *Nat. Commun.* **9**, 1324 (2018).
45. Sprintall, J., Cravatte, S., Dewitte, B., Du, Y. & Gupta, A. S. In *El Niño Southern Oscillation in a Changing Climate* (eds McPhaden, M. J., Santoso, A. & Cai, W.) (John Wiley & Sons, Inc., 2020).
46. Amaya, D. J. et al. Subseasonal-to-seasonal forecast skill in the California Current System and its connection to coastal Kelvin waves. *J. Geophys. Res. Oceans* **127**, e2021JC017892 (2022).
47. Capotondi, A. & Qiu, B. Decadal variability of the Pacific shallow overturning circulation and the role of local wind forcing. *J. Clim.* **36**, 1001–1015 (2023).
48. Chen, K. & Kwon, Y.-O. Does Pacific variability influence the Northwest Atlantic shelf temperature? *J. Geophys. Res. Oceans* **123**, 4110–4131 (2018).
49. Zhang, L. & Delworth, T. L. Analysis of the characteristics and mechanisms of the Pacific decadal oscillation in a suite of coupled models from the geophysical fluid dynamics laboratory. *J. Clim.* **28**, 7678–7701 (2015).
50. Zhang, L. & Delworth, T. L. Simulated response of the Pacific decadal oscillation to climate change. *J. Clim.* **29**, 5999–6018 (2016).
51. Li, S. et al. The Pacific Decadal Oscillation less predictable under greenhouse warming. *Nat. Clim. Change* **10**, 30–34 (2020).
52. Capotondi, A., Alexander, M. A., Bond, N. A., Curchitser, E. N. & Scott, J. D. Enhanced upper ocean stratification with climate change in the CMIP3 models. *J. Geophys. Res.* **117**, C04031 (2012).
53. Liu, Z. Dynamics of interdecadal climate variability: a historical perspective. *J. Clim.* **25**, 1963–1995 (2012).
54. Newman, M. et al. The Pacific decadal oscillation, revisited. *J. Clim.* **29**, 4399–4427 (2016).
55. Liu, Z. & Di Lorenzo, E. Mechanisms and predictability of Pacific decadal variability. *Curr. Clim. Change Rep.* **4**, 128–144 (2018).
56. Jacox, M. G., Tommasi, D., Alexander, M. A., Hervieux, G. & Stock, C. A. Predicting the evolution of the 2014–2016 California Current System marine heatwave from an ensemble of coupled global climate forecasts. *Front. Mar. Sci.* **6**, 497 (2019).
57. Jacox, M. G. et al. Global seasonal forecasts of marine heatwaves. *Nature* **604**, 486–490 (2022).
58. Huang, B. et al. Improvements of the Daily Optimum Sea Surface Temperature (DOISST)—version 2.1. *J. Clim.* **34**, 2923–2939 (2021).
59. Ishii, M., Shouji, A., Sugimoto, S. & Matsumoto, T. Objective analyses of sea-surface temperature and Marine meteorological variables for the 20th century using ICOADS and the Kobe collection. *Int. J. Climatol.* **25**, 865–879 (2005).
60. Hirahara, S., Ishii, M. & Fukuda, Y. Centennial-scale sea surface temperature analysis and its uncertainty. *J. Clim.* **27**, 57–75 (2014).
61. Huang, B. et al. Extended reconstructed sea surface temperature, version 5 (ERSSTv5): upgrades, validations, and intercomparisons. *J. Clim.* **30**, 8179–8205 (2017).
62. Rayner, N. A. et al. Global analyses of sea surface temperature, sea ice, and night marine air temperature since the late nineteenth century. *J. Geophys. Res. Atmos.* **108**, 4407 (2003).
63. Deser, C., Alexander, M. A., Xie, S.-P. & Phillips, A. S. Sea surface temperature variability: patterns and mechanisms. *Ann. Rev. Mar. Sci.* **2**, 115–143 (2010).
64. Meehl, G. A., Hu, A. & Tebaldi, C. Decadal prediction in the Pacific region. *J. Clim.* **23**, 2959–2973 (2010).
65. Ding, R., Li, J., Zheng, F., Feng, J. & Liu, D. Estimating the limit of decadal-scale climate predictability using observational data. *Clim. Dyn.* **46**, 1563–1580 (2016).
66. Ziehn, T. et al. The Australian earth system model: ACCESS-ESM1. 5. *J. South. Hemisphere Earth Syst. Sci.* **70**, 193–214 (2020).
67. Swart, N. C. et al. The Canadian earth system model version 5 (CanESM5.0.3). *Geosci. Model Dev.* **12**, 4823–4873 (2019).
68. Kay, J. E. et al. The Community Earth System Model (CESM) large ensemble project: a community resource for studying climate change in the presence of internal climate variability. *Bull. Am. Meteorol. Soc.* **96**, 1333–1349 (2015).
69. Rodgers, K. B. et al. Ubiquity of human-induced changes in climate variability. *Earth Syst. Dyn.* **12**, 1393–1411 (2021).
70. Capotondi, A., Deser, C., Phillips, A. S., Okumura, Y. & Larson, S. M. ENSO and Pacific decadal variability in the community earth system model version 2. *J. Adv. Model. Earth Syst.* **12**, e2019MS002022 (2020).
71. Döschner, R. et al. The EC-Earth3 earth system model for the coupled model intercomparison project 6. *Geosci. Model Dev.* **15**, 2973–3020 (2022).
72. Liu, W., Xie, S.-P. & Lu, J. Tracking ocean heat uptake during the surface warming hiatus. *Nat. Commun.* **7**, 10926 (2016).
73. Hobday, A. J. et al. A hierarchical approach to defining marine heatwaves. *Prog. Oceanogr.* **141**, 227–238 (2016).
74. Ren, X. & Liu, W. The role of a weakened Atlantic meridional overturning circulation in modulating marine heatwaves in a warming climate. *Geophys. Res. Lett.* **48**, e2021GL095941 (2021).

Acknowledgements

We would like to thank the two anonymous reviewers whose comments have helped us to significantly improve the manuscript. This work is supported by grants to W.L. from U.S. National Science Foundation (AGS-2053121, OCE-2123422 and AGS-2237743). W.L. is also supported by the Hellman Fellows Fund as a Hellman Fellow. N.J.H. acknowledges funding support from the ARC Centre of Excellence for Climate Extremes (CE170100023) and the National Environmental Science Program Climate Systems Hub. A.C. was supported by the NOAA Climate Program Office Modeling Analysis Prediction and Projection (MAPP) Program.

Author contributions

W.L. conceived the study. X.R. performed the analysis. X.R. and W.L. wrote the original draft of the manuscript. A.C., D.J.A. and N.J.H. contributed to interpreting the results and made substantial improvements to the manuscript.

Competing interests

The authors declare no competing interests.

Additional information


Supplementary information The online version contains supplementary material available at <https://doi.org/10.1038/s43247-023-00863-w>.

Correspondence and requests for materials should be addressed to Xianglin Ren.

Peer review information *Communications Earth & Environment* thanks the anonymous reviewer(s) for their contribution to the peer review of this work. Primary Handling Editors: Heike Langenberg. A peer review file is available.

Reprints and permission information is available at <http://www.nature.com/reprints>

Publisher's note Springer Nature remains neutral with regard to jurisdictional claims in published maps and institutional affiliations.

 **Open Access** This article is licensed under a Creative Commons Attribution 4.0 International License, which permits use, sharing, adaptation, distribution and reproduction in any medium or format, as long as you give appropriate credit to the original author(s) and the source, provide a link to the Creative Commons license, and indicate if changes were made. The images or other third party material in this article are included in the article's Creative Commons license, unless indicated otherwise in a credit line to the material. If material is not included in the article's Creative Commons license and your intended use is not permitted by statutory regulation or exceeds the permitted use, you will need to obtain permission directly from the copyright holder. To view a copy of this license, visit <http://creativecommons.org/licenses/by/4.0/>.

© The Author(s) 2023